Shear and ductility assessment of a prefabricated thermal break system for internally insulated buildings

Mohammad Abdallah[1], Hugues Somja[1]

[1] *INSA Rennes, LGCGM Structural Engineering Research Group, 20 avenue des Buttes de Coesmes, CS 70839, Rennes Cedex 7 F-35708, France*

ABSTRACT Prefabricated thermal break systems (PTBSs) for external reinforced concrete (RC) joints have been demonstrated to improve the thermal performance of internally insulated buildings. Despite the heat-loss protection, critical discussion remains on the potential of PTBSs to transfer shear and bending forces between RC members to achieve the ductility and strength required for safe seismic design. This study experimentally investigates the hysteretic response of three large-scale wall-slab joints constructed with a proposed PTBS called SLABE-Z8, with particular attention to the shear and energy dissipation capacities. The tested specimens showed sufficient strength, ductility, and ability to dissipate energy in the post-yielding zone, highlighting the potential of SLABE-Z8 in resolving shear strength and design provision issues of insulated joints in earthquake-prone areas.

Key words SLABE, thermal, cyclic, shear, ductility, stiffness

I. INTRODUCTION

External insulation is commonly used in buildings and apartment blocks, but it can be expensive and vulnerable to damage caused by weather and external accidents (Dionysios et al., 2013). Research has shown that internal insulation can be 7%–19% more effective in areas that experience hot summers and cold winters (Xiaolong et al., 2017; Xi et al., 2018). Nevertheless, internal insulation can create thermal bridges at exterior connections, significantly reducing the building's thermal performance. Thermal bridges can result from geometric configurations, material disparities, or their combinations (Theodosiou et al., 2008). In buildings, it is often related to specific design or construction elements. Heat loss due to thermal bridges or weak points in the thermal envelope can exceed 30% of the total heat lost in a building (Evola et al., 2011). Moreover, it may influence the structural members' materials, resulting in material damage (~40% in walls) due to moisture condensation (Ali et al., 2022), thus increasing maintenance repair costs.

Prefabricated or manufactured structural thermal breaks (PTBSs) are a solution for interrupting thermal loss and ensuring the continuity of the internal insulation material at the thermal bridging location. Several types of PTBSs, such as Isokorb (2016), Armatherm FRR (2016), and Farrat TBK/TBL (2020), have been introduced and used in the construction industry. PTBSs are similar to thermal break pads or plates (Ben Larbi et al., 2022; Salih et al., 2020); however, they generally incorporate a structural system that allows transfer bending and axial stresses. Under seismic or lateral actions, the PTBSs must transmit the shear forces and ensure the rigidity of a joint with sufficient ductility and energy absorption capacity, which research studies have not been conducted until recently, particularly for exterior wall-slab joints. In general, existing commercial PTBSs can provide joints with limited vertical and horizontal shear capacities, which can be attributed to their minimal structural system that consists only of steel bars. Consequently, a new type of PTBS for exterior wall–slab connections, called SLABE, was developed by

COHB-industrie (2023) in collaboration with INSA-Rennes. The SLABE system uses steel profiles (Z or N) and stainless-steel bars to transfer shear, bending, and axial forces. Incorporating an arrangement of Z and N profiles in SLABE-ZN was previously investigated (Gaël et al., 2016), and the results highlighted its high shear capacity, approximately 120.5 kN/m under vertical loading and 190.2 kN/m under horizontal loading, allowing for its use as a non-dissipative element in earthquake-prone areas. Nevertheless, this initial system was over-resistant in many cases. Therefore, the present study evaluates the ability of Z profiles and steel bars in a new arrangement, called SLABE-Z8, to dissipate energy by examining its hysteretic response, failure mode, ductility, and energy dissipation capacity.

II. EXPERIMENTAL PROGRAM, MATERIAL PROPERTIES, AND LOADING PROTOCOL

A. Description of SLABE-Z8

SLABE-Z8 is a thermal break developed by COHB-industrie. Its purpose is to prevent heat transfer at the thermal bridging location, particularly at the exterior connections, and to improve the overall thermal performance of the building envelope. Thus, the structural system of SLABE-Z8 must ensure structural safety by providing sufficient rigidity to withstand horizontal and vertical loads. Each unit of SLABE-Z8 measures 1000 mm in length and 85 mm in thickness. It consists of a thick layer of mineral wool as an insulation material, four U-shaped steel bars (Ø8 mm) spaced 250 mm center-to-center, and one Z-profile (3 mm thickness, 50 mm flange width, and 100 mm height), as shown in Figure 1. Schematically, the U-steel bars transfer the bending moment, and the Z profile ensures the transfer of shear forces. The Z-profile and U-steel bars were made of stainless steel with a limit of elasticity greater than 358 and 717 MPa, respectively. The thermal conductivities of the insulation material and stainless steel were 0.038 (W/m.K) and 14.61 (W/m.K) (Eurocode 3, 1993), respectively. The use of mineral wool and stainless steel in SLABE-Z8 resulted in good thermal performance with an effective thermal transmittance of less than 0.27 (W/m.K) (Keo et al., 2018).

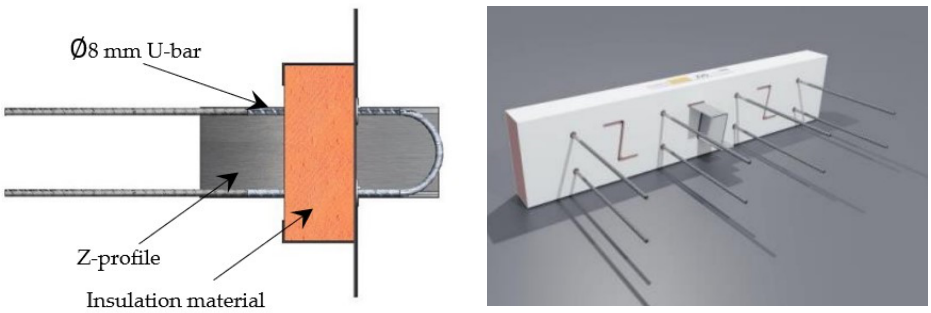

(a) Components (b) 3D-View

Figure 1. SLABE-Z8

B. Tested specimen and material properties

To verify the behavior of the SLABE-Z8 system, three identical large-scale specimens using concrete C25/30 were tested, each consisting of a reinforced concrete (RC) wall and slab. The test program provides data redundancy and complies with the standards for determining the design capacity. The wall and slab, including the steel reinforcement, were constructed in accordance with the recommendation of Eurocode-2 (2004), Eurocode-8 (2004), and the TBS production. The SLABE-Z8 system was employed at the wall-to-slab connection. The wall dimensions were 1.80 m in height, 1.00 m in width, and 0.16 m in thickness, and the slab dimensions were 1.372 m in length, 1.00 m in width, and 0.20 m in thickness. Each specimen was subjected to vertical constant load (37 kN) and cyclic reversed load. The vertical load was applied at approximately 100 mm from the interior face of the wall

and was transferred to the RC slab by a steel setup, ensuring that it was outside the critical shear zone of the SLABE-Z8. The cyclic loads were applied to the concrete slab at approximately 405 mm from the interior face of the wall. Two LVDTs with a capacity of 100 mm were used to measure the relative displacement of the SLABE-Z8 with respect to the exterior wall. The LVDTs were placed 150 mm from the interior face of the wall. Figure 2 shows the general test setup, including specimen dimensions, loading, supporting mechanism, and LVDTs locations. In addition, Table 1 summarizes the compressive strength of the used concrete on the day of the tests (age >28 days).

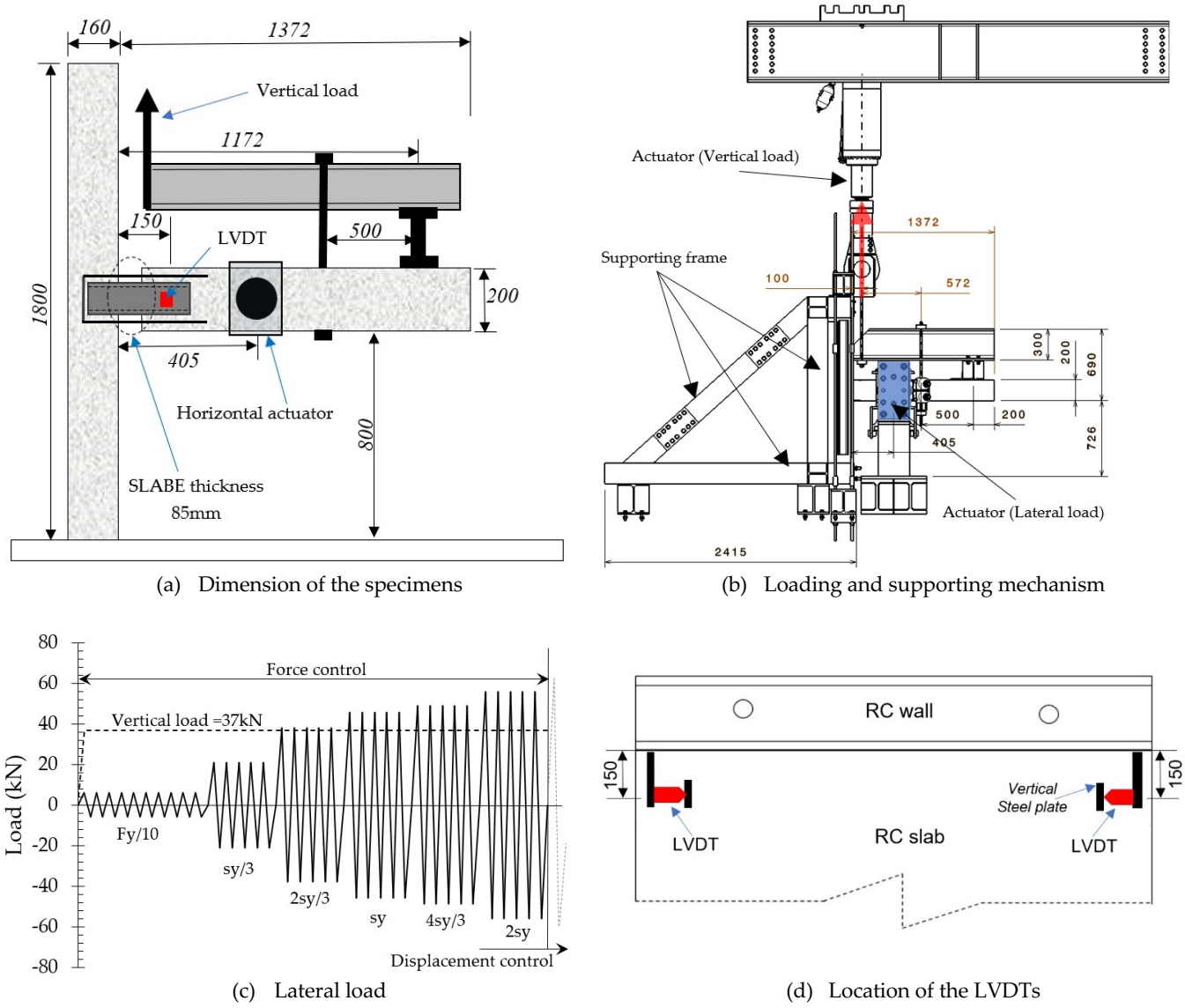

(a) Dimension of the specimens

(b) Loading and supporting mechanism

(c) Lateral load

(d) Location of the LVDTs

Figure 2. Dimensions and **test setup (Dimensions in mm)**

Table 1. Concrete average compressive strength

Specimen	Wall (MPa)	Slab (MPa)	Average (MPa)
CHT-1	31.19	29.57	30.38
CHT-2	37.18	28.33	32.76
CHT-3	33.99	29.71	31.85

C. Loading protocol

The loading protocol is presented in Figure 2c. It was built on the basis of the static yielding displacement (s_y = 2.5 mm). The static yielding displacement was determined by testing another specimen under a monotonic increasing horizontal load; however, the results are not presented in this paper. The loading protocol of the CHT specimens was divided into two stages based on the imposed loading type (i.e., force or displacement). The force-imposed stage comprises six loading periods (up to $2s_y$), and the displacement-imposed stage comprises at least three loading periods (ns_y, where n = 3, 4, 5 ...etc.). The number of cycles in each loading period was greater than 3 to comply with Eurocod-8 (2004). The vertical load (37 kN), representing the dead and live loads, was kept constant throughout the test.

III. RESULTS AND DISCUSSION

This section discusses the results of the CHT specimens regarding their hysteretic response, failure mode, stiffness degradation, and energy dissipation capacity. In addition, Table 2 presents the main results obtained from the tests in terms of yielding load (F_y), maximum load (F_{max}), ultimate load (F_u), and displacement ductility index (μ), Eq.1. The yielding load (F_y) was determined using the Aribert and Lachal approach (Aribert & Lachal, 2002).

Table 2. Main results of the CHT specimens

Specimen	Force (1)	F_y (2)	s_y (3)	F_{max} (4)	F_u (5)	S_u (6)	μ (7)	μ_{avg} (8)
CHT-1	Pushing	54.9	2.55	57.9	55.2	17.30	6.78	5.96
	Pulling	60.0	3.10	61.8	52.8	15.90	5.13	
CHT-2	Pushing	53.0	2.50	60.9	52.9	17.46	6.98	6.54
	Pulling	62.0	2.95	65.5	56.3	17.98	6.09	
CHT-3	Pushing	56.0	2.50	61.9	56.7	17.28	6.91	5.90
	Pulling	60.5	3.70	63.3	56.4	16.94	4.80	

(1) Pushing is the positive loading, and pulling is the negative loading; (2)F_y is the yielding load (kN); (3) s_y is the yielding displacement (mm). (4) F_{max} is the maximum load (kN); (5) F_u is the ultimate load, which is equal to either 0.85F_{max} or the load at the end of the test (whichever comes first); (6) S_u is theultimate displacement (mm) corresponding to F_u; (7) μ is theductility index; and (8) μ_{avg} is the average ductility index.

A. Hysteretic response

Figure 3 shows the hysteretic response of each specimen. As expected, the response was very similar because all specimens had the same material and dimensions and were subjected to nearly the same loading protocol. The yielding load (F_y) ranged between 53 and 56 kN under positive loading (pushing) and between 60 and 62 kN under negative loading (pulling). Similarly, the maximum load (F_{max}) ranged between 57.9 and 61.9 kN under positive loading and 61.8 and 65.5 kN under negative loading.

B. Failure mode

Figure 4 shows the failure mode observed in the three tests and the buckling deformation of the Z profiles. The SLABE-Z8 attained maximum carrying capacity when punching in the concrete floor occurred in the eighth loading period ($4s_y$). This was followed by decreased system capacity, mainly due to decreased connection stiffness. The SLABE-Z8 system could resist horizontal cyclic loading in

the degradation zone until fracture and/or severe buckling in the Z profile was formed. Indeed, fracture or buckling of the Z flanges was observed in all CHT specimens at the end of the tests ($7s_y$).

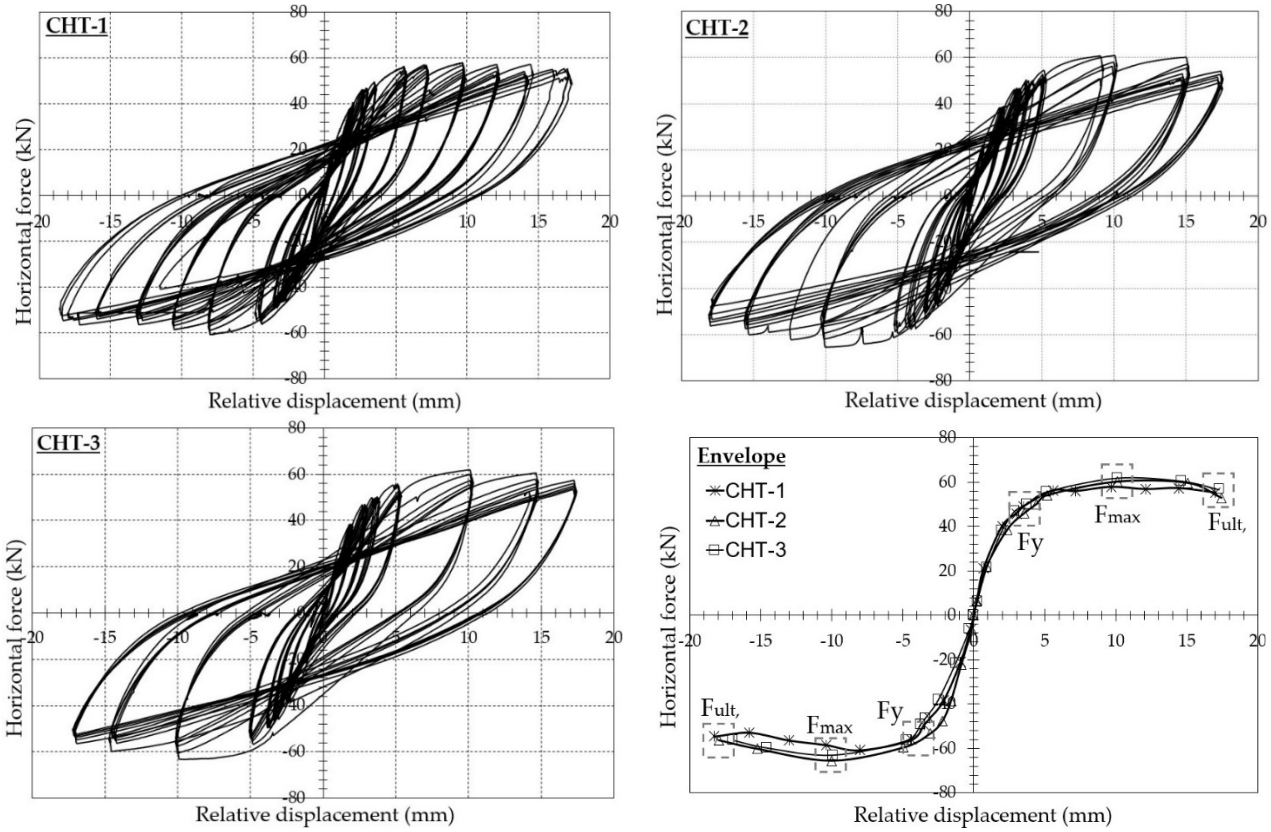

Figure 3. Hysteretic response of tested specimens

C. Ductility performance

The ductility of a structure refers to its ability to absorb energy by undergoing plastic deformation before collapse. The ductility index (μ) was used to evaluate the ductility performance of the tested CHTs. It is obtained on the basis of displacement computation, as given in Eq. 1, where s_y and s_{ult} are the displacement at the yielding and ultimate load levels, respectively. As can be seen from Table 2, the CHT specimens exhibited a satisfactory level of ductility in the positive and negative loadings, with an average ranging between 5.90 and 6.54.

$$\mu = \frac{s_y}{s_{ult}} \tag{1}$$

D. Stiffness degradation and post-peak softening

The peak-to-peak stiffness (K_{secant}) of the CHT specimens, expressed in kN/mm, was calculated for each loading period based on the slope of the line connecting the maximum positive (F^+_{max}) and negative (F^-_{max}) load values of the first cycle of each loading period, as given in Eq. 2. The obtained stiffness values are presented in Table 3. In addition, Figure 5 illustrates the stiffness degradation versus the relative displacement.

$$K_{secant} = \frac{|F_{max}^{+}| + |F_{max}^{-}|}{|s_i^{+} + s_i^{-}|} \quad (2)$$

where, F_{max}^{+} is the maximum positive load, F_{max}^{-} is the maximum negative load, s_i^{+} is the maximum positive displacement, and s_i^{-} is the maximum negative displacement.

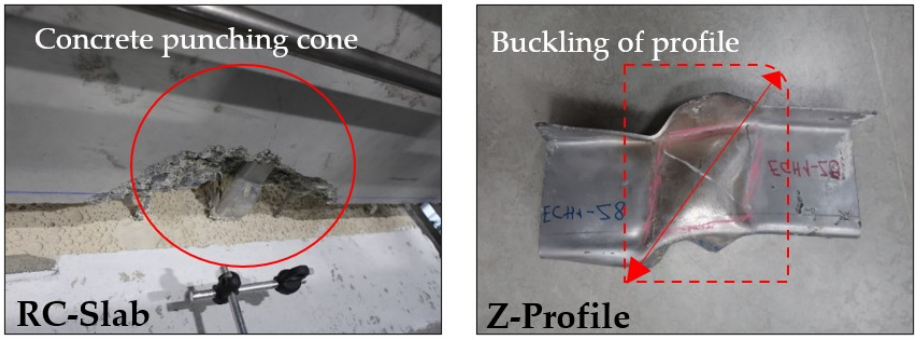

(a) CHT-1

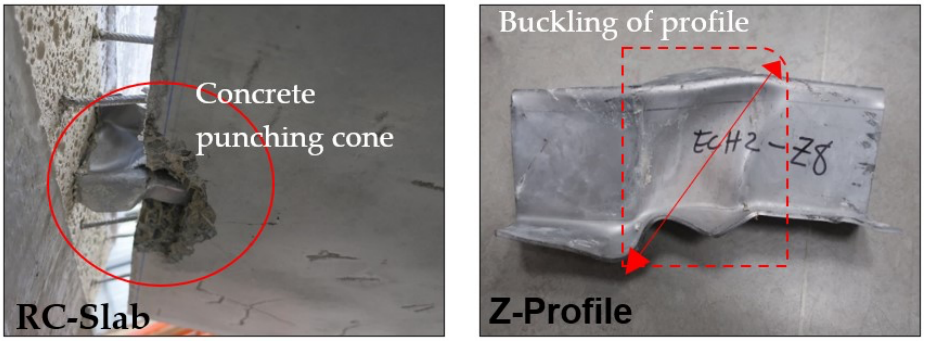

(b) CHT-2

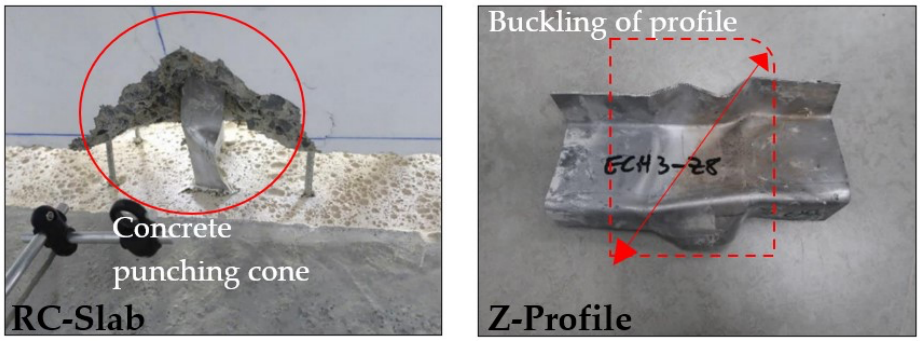

(c) CHT-3

Figure 4. Failure mode of tested specimens

As shown in Figure 5 and Table 3, the stiffness decreases with increasing relative displacement, in an exponential form, with a relatively low degradation rate ($K_{secant} = 21.294e^{-0.114s}$). In the first loading period ($\frac{F_y^-}{10}, \frac{F_y^+}{10}$), CHT-1, CHT-2, and CHT-3 exhibited stiffness values of 30.23, 35.68, and 22.91 kN/mm, respectively, whereas in the last loading period ($\frac{s_y^-}{7}, \frac{s_y^+}{7}$), the stiffness values were 3.11, 3.08, and 3.31 kN/mm, respectively. This implies that the degradation percentage in stiffness between the first and last loading periods was approximately 89.71% in CHT-1, 91.37% in CHT-2, and 85.55% in CHT-3. However, CHT-1, CHT-2, and CHT-3 achieved average stiffness values of 12.75, 15.05, and 12.55 kN/mm, respectively.

The post-peak softening (S, kN/mm) indicates the structural behavior and residual strength after the maximum load was reached. The structural behavior characteristics of the CHT specimens after the maximum load (i.e., in the post-peak zone) were determined by dividing the difference between the ultimate force (F_u) and the maximum load (F_{max}) by the difference between their corresponding displacements (s_u^+, s_{max}^+), as given in Eq. 3. Thus, the S values of CHT-1, CHT-2, and CHT-3 were found to be -0.35, -1.09, and -0.72 kN/mm, respectively, under the positive loading (pushing) and -1.14, -1.15, and -0.98 kN/mm under the negative loading (pulling).

$$S = \frac{|F_u^+| - |F_{max}^+|}{|s_u^+ - s_{max}^+|} \quad (3)$$

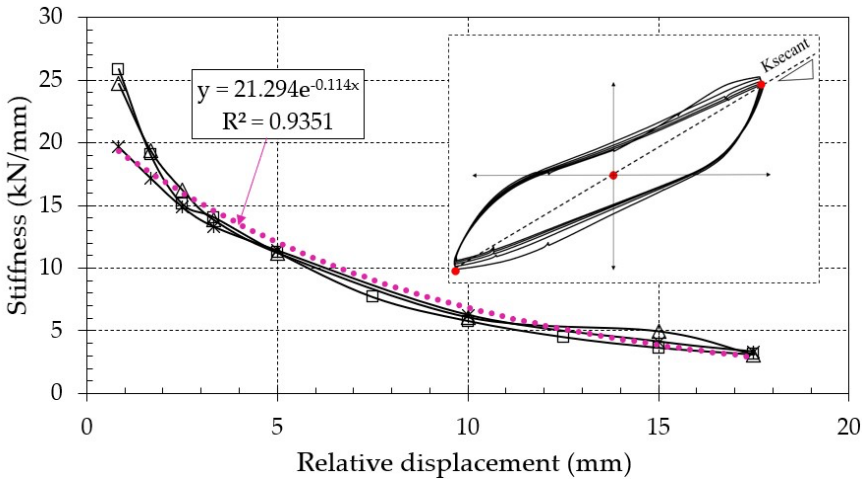

Figure 5. Stiffness vs. relative displacement of CHT specimens

Table 3. Stiffness of the CHT specimens

Loading step (1)	Displacement or load level	CHT-1	CHT-2	CHT-3	Average (5) kN/mm
		K_{secent} (2) kN/mm	K_{secent} kN/mm	K_{secent} kN/mm	
1	$F_y/10$	30.23	35.68	22.91	29.61
2	$s_y/3$	25.87	24.74	19.66	23.42
3	$2s_y/3$	19.04	19.42	17.18	18.55
4	s_y	15.11	16.25	14.86	15.41
5	$4s_y/3$	14.04	13.84	13.29	13.72
6	$2s_y$	11.23	11.21	11.39	11.28
7	$3s_y$	7.68	------(3)	------(3)	7.68
8	$4s_y$	5.78	6.25	6.25	6.09
9	$5s_y$	4.50	------(3)	------(3)	4.50
10	$6s_y$	3.64	4.94	4.12	4.23
11	$7s_y$	3.11	3.08	3.31	3.17
Degradation (4)	------	89.71%	91.37%	85.55%	------
Average (5)	------	12.75	15.05	12.55	13.45

(1) See Figure 2c ; (2) K_{secent} is secent stiffness calculated at the end of each loading period; (3) The specimen was not tested for this loading period; (4) Degradation (%) = $\frac{K_{secent}(last) - K_{secent}(intial)}{K_{secent}(intial)} \times 100\%$; and (5) Average = $\frac{\sum K_{secent}}{n}$.

E. Energy dissipation capacity and damping ratio

The two main criteria for the seismic design of structures are strength and ductility. Regarding the latter, RC and composite structures dissipate energy by experiencing high deformation or inelastic behavior. The energy dissipation (E_d) of the CHTs was computed for each loading period based on the area enclosed inside the absolute hysteresis loop, as shown in Figure 6 and given in Eq. 4. However, a structure resisting cycle loading develops damping in the inelastic region, which increases as the displacement increases. Therefore, the damping ratio (ζ_{eq}) was calculated (Eq. 5) and is presented in Table 4.

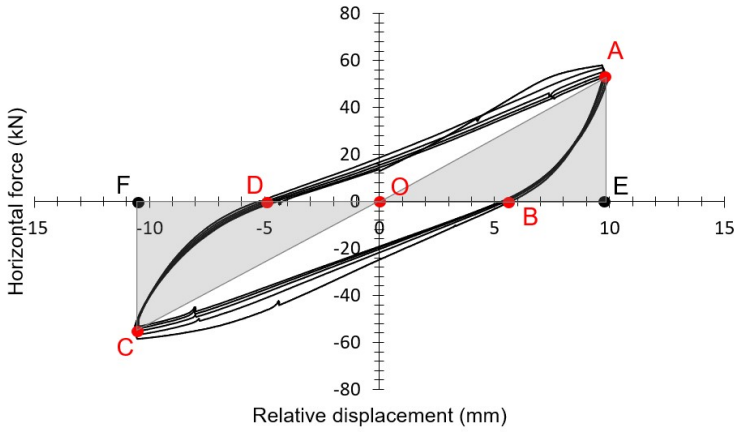

Figure 6. Energy dissipation profile

$$E_d = Area(ABCD) \tag{4}$$

$$\zeta_{eq} = \frac{E_d}{2\pi \times (Area(OAE) + Area(OCF))} \tag{5}$$

Overall, the energy dissipation capacity and damping ratio of the CHTs were very close to each other. As can be seen from Table 4, the average energy dissipation capacities of CHT-1, CHT-2, and CHT-3 were 438.19, 415.73, and 441.18 kN.mm, respectively, and the average damping ratio was 0.15, 0.14, and 0.14, respectively. As shown in Figure 7, one the other hand, the cumulative amount of dissipated energy was negligible up to the yielding level, accounting for only 3.11%–4.53% of the total cumulative value. This indicates that the SLABE-Z8 system dissipates 95.15%–96.89% of energy in the post-yielding region or after plastic hing formation, signifying its applicability for joints in earthquake-prone areas.

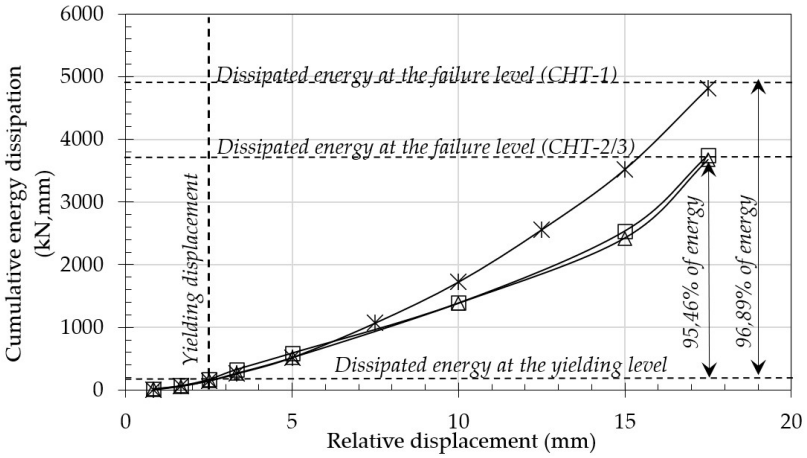

Figure 7. Energy dissipation capacity of the SLABE-Z8 system

Table 4. Energy dissipation capacity and damping ratio of CHT specimens

Loading step (1)	CHT-1		CHT-2		CHT-3		E_d (4) Average	ζ_{eq} (4) Average
	E_d (2) kN.mm	ζ_{eq} (3)	E_d kN.mm	ζ_{eq}	E_d kN.mm	ζ_{eq}		
1	0.43	0.05	0.28	0.05	0.78	0.07	0.50	0.06
2	9.47	0.09	17.67	0.14	11.71	0.09	12.95	0.11
3	54.14	0.11	52.8	0.11	45.40	0.09	50.78	0.10
4	86.34	0.10	99.26	0.12	84.22	0.09	89.94	0.10
5	112.6	0.11	159.0	0.13	121.0	0.11	130.87	0.12
6	258.1	0.15	260.6	0.14	248.10	0.15	255.60	0.15
7	552.0	0.21	------	------	------	------	552.00	0.21
8	653.4	0.18	799.0	0.21	869.1	0.22	773.83	0.20
9	834.5	0.19	------	------	------	------	834.50	0.19
10	963.1	0.19	1147.0	0.21	1042.0	0.20	1050.70	0.20
11	1296.0	0.22	1206.0	0.20	1248.0	0.20	1250.00	0.21
Average (4)	438.19	0.15	415.73	0.14	441.18	0.14	446.7	0.14

(1) See Figure 2c ; (2) E_d is the energy dissipation capacity; (3) ζ_{eq} is the damping ratio; and (4) Average = $\frac{\sum E_d \text{ or } \zeta_{eq}}{n}$.

F. Behavior factor of CHTs for seismic design

The behavior factor (q) introduced in Eurocode-8 (2004) accounts for the energy dissipation capacity of a structure. For a dissipative structure such as a composite or concrete wall coupled by a steel or composite beam, the upper limit of q should be taken as $3\alpha_u/\alpha_1$ for medium ductility class (DCM) and 4.5 α_u/α_1 for high ductility class (DCH), where α_u and α_1 are the seismic load that causes the complete plastic mechanism and that at the formation of the first yielding hinge, respectively. Given that α_u/α_1 ranges between 1.2 and 1.3, the q value of the dissipative structures ranges between 3.6 and 3.9 for DCM and between 5.4 and 5.85 for DCH.

According to Eurocode 8, the selection of the behaviour factor is one of the initial steps in designing a building for seismic load. It can be estimated or evaluated based on the experimental envelope response (Villani et al., 2009), as demonstrated in Figure 8 and Eq. 6, where F_e and F_y are the elastic response strength and yielding strength of the idealized response, respectively, and the term q_u refers to the amount of energy that a structure can dissipate through its hysteretic response.

Although the behavior factor is a parameter of a building as a whole, it is interesting to compute its value for subsystems to give a qualitative evaluation of their ductility. The behavior factor (q) of the CHT specimens are presented in Table 5. The q values were found to be around 4, indicating that the SLABE Z8's ductility can be categorized in the medium range.

$$q = \frac{F_e^{max}}{F_{el}} = \frac{F_e^{max}}{F_y} \times \frac{F_y}{F_{el}} = q_u \times \alpha_u/\alpha_1 \quad (6)$$

Table 5. Behavior factor of CHTs

Specimen	F_e^{max}	F_y	q_u
CHT-1	226	54.9	4.12
CHT-2	218	53	4.11
CHT-3	220	56	3.93

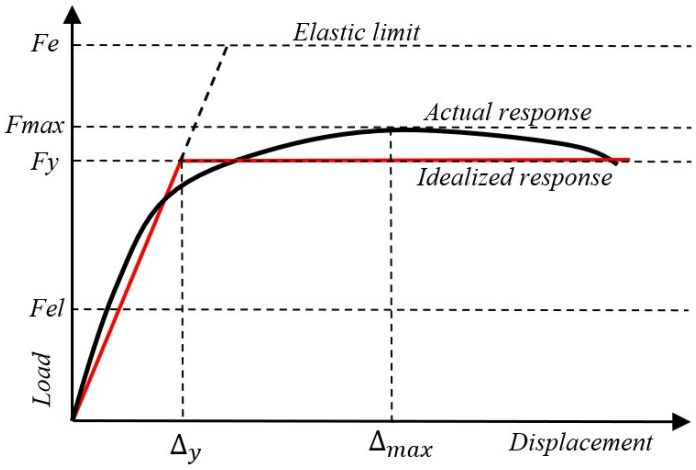

Figure 8. Load vs. displacement response (Villani et al., 2009)

IV. CONCLUSION AND RECOMMENDATIONS

This study aimed to evaluate the structural performance of a new type of PTBS, SLABE-Z8, by conducting tests on three specimens subjected to horizontal reversed cyclic loading. Compared to the existing PTBSs, and drawing from the experimental results, SLABE-Z8 exhibited satisfactory ductility (μ_{avg} = 6.13), shear capacity (F_{avg}^{max+} 60.23 kN/m, F_{avg}^{max-} = 60.53 kN/m), and stiffness (K_{avg}= 13.45 kN/mm) despite the concrete punching failure mode. Furthermore, based on the energy dissipation analysis and behavior factor evaluation of the hysteretic and envelope curves, SLABE-Z8 could dissipate energy in the inelastic response, making it a promising solution for thermal and mechanical use at the exterior wall–slab connections of internally insulated buildings.

In conclusion, SLABE-Z8 is proposed for potential use in buildings located in low-moderate seismic areas. Nevertheless, further studies based on dynamic and base shear analysis are required to verify the gain in energy dissipation performance and the behavior factor of buildings employing SLABE-Z8 in the structural envelopes.

V. ACKNOWLEDGEMENTS

The authors gratefully acknowledge financial support from the French National Research Agency (ANR, Paris) and INGENOVA with grant number ANR-21-CHIN-0003 through the ANR FREEINBTP project.

REFERENCES

Dionysios I. Kolaitis, Emmanouil Malliotakis, Dimos A. Kontogeorgos, Ioannis Mandilaras, Dimitrios I. Katsourinis, Maria A. Founti. (2013). Comparative assessment of internal and external thermal insulation systems for energy efficient retrofitting of residential buildings. Energy and Buildings (64) 123–131.

Xiaolong Wang, Li He, Qilin Wang. (2017). Influence of insulation layer position on short-time intermittent heating room, Procedia Eng. (205) 1484–1493. https://doi.org/10.1016/j.proeng.2017.10.374.

Xi Meng, Tao Luo, Yanna Gao, Lili Zhang, Huang Xing, Chaoping Hou, Qiong Shen, Enshen Long. (2018). Comparative analysis on thermal performance of different wall insulation forms under the air-conditioning intermittent operation in summer, Appl. Therm. Eng. (130) 429–438, https://doi.org/10.1016/j. applthermaleng.2017.11.042.

T.G. Theodosiou, A.M. Papadopoulos. (2008). The impact of thermal bridges on the energy demand of buildings with double brick wall constructions, Energy Build. 40 (11) 2083–2089, https://doi.org/10.1016/j. enbuild.2008.06.006.

G. Evola, G. Margani, L. Marletta. (2011). Energy and cost evaluation of thermal bridge correction in Mediterranean climate, Energy Build. 43 (9) 2385–2393, https://doi.org/10.1016/j.enbuild.2011.05.028.

Ali El Saied, Chadi Maalouf, Timea Bejat, Etienne Wurtz. (2022). Slab-on-grade thermal bridges: A thermal behavior and solution review. Energy & Buildings (257) 111770.

USA Inc. (2016). Thermal Bridge Solutions. Schöck Isokorb Product Guide. Guide to Thermal Breaks . Innovative Design in Practice. Schöck USA Inc., New York, NY.

Armadillo Noise & Vibration Ltd. (2016). Thermal Break Pads Armatherm Grade FR - Ultra High Strength, High Performance. Armadillo Noise & Vibration Ltd., Shipley, West Yorkshire, England.

Farrat. (2020). Thermal Break Connections (Farrat). Farrat.

A. Ben Larbi, M. Couchaux, C. Thauvoye, C. Sautot. (2022). Mechanical and fire tests on thermal breaks attached to concrete supports. Journal of Constructional Steel Research (190) 107114.

Salih Qasim Mahmood, Thomas Schumacher, Peter Dusicka, Hormoz Zareh. (2020). Structural behavior of bolted steel lap shear connections with thermally insulating filler plates. Journal of Constructional Steel Research (167). 105852.

COHB-Industrie. (2023). SLABE-thermal break system. France.

Gaël Le Bloa, Hugues Somja, Franck Palas. (2016). Experimental Study on the Seismic Behaviour of an Innovative Hybrid Concrete Connection Used as Thermal Break System. Key Engineering Materials (711). 1019-1026. https://doi.org/10.4028/www.scientific.net/KEM.711.1019

Eurocode 3. (1993). Design of steel structures - Part 1-2: General rules - Structural fire design.

Keo, P., Le Gac, B., Somja, H., Palas, F. (2018). Experimental Study of the Behavior of a Steel-Concrete Hybrid Thermal Break System Under Vertical Actions. In: Hordijk, D., Luković, M. (eds) High Tech Concrete: Where Technology and Engineering Meet. Springer, Cham. https://doi.org/10.1007/978-3-319-59471-2_293.

Eurocode 2. (2004). Design of concrete structures - Part 1-1: General rules and rules for buildings.

Eurocode 8. (2004). Design of structures for earthquake resistance – Part 1: General rules, seismic actions and rules for buildings. European Committee for Standardization (CEN), Brussels, Belgium.

J.-M. Aribert and A. Lachal. (2022). Formulation de la rupture par fatigue de connecteurs acier-béton pour des sollicitations de type sismique: Application aux assemblages. Construction métallique, 39(4) :3–11. [In French].

Villani, A., Castro, J.M. and Elghazouli, A.Y. (2009). Improved seismic design procedure for steel moment frames", Proceedings of the 6th International Conference Stessa-2009, behaviour of Steel Structures in Seismic Areas, Philadelphia, PA, USA, August, pp. 673-678.